



**HAL**  
open science

## Conductivity vs functionalization in single-walled carbon nanotube films

Mohammad Jouni, Pavol Fedorko, Caroline Celle, David Djurado, Pascale Chenevier, Jerome Faure-Vincent

► **To cite this version:**

Mohammad Jouni, Pavol Fedorko, Caroline Celle, David Djurado, Pascale Chenevier, et al.. Conductivity vs functionalization in single-walled carbon nanotube films. SN Applied Sciences, 2022, 4 (4), pp.132. 10.1007/s42452-022-05016-w . hal-03629750

**HAL Id: hal-03629750**

**<https://hal.science/hal-03629750v1>**

Submitted on 23 Aug 2024

**HAL** is a multi-disciplinary open access archive for the deposit and dissemination of scientific research documents, whether they are published or not. The documents may come from teaching and research institutions in France or abroad, or from public or private research centers.

L'archive ouverte pluridisciplinaire **HAL**, est destinée au dépôt et à la diffusion de documents scientifiques de niveau recherche, publiés ou non, émanant des établissements d'enseignement et de recherche français ou étrangers, des laboratoires publics ou privés.



Distributed under a Creative Commons Attribution 4.0 International License




# Conductivity vs functionalization in single-walled carbon nanotube films

Mohammad Jouni<sup>1</sup> · Pavol Fedorko<sup>2</sup> · Caroline Celle<sup>3</sup> · David Djurado<sup>1</sup> · Pascale Chenevier<sup>1</sup> · Jérôme Faure-Vincent<sup>1</sup> 

Received: 21 January 2022 / Accepted: 14 March 2022

Published online: 01 April 2022

© The Author(s) 2022 

## Abstract

Diazo functionalization is a chemical method that changes the conductance of metallic single-walled carbon nanotubes (SWCNTs) by disrupting the C–C double bonds. Its application to native mixtures of metallic and semiconducting SWCNTs is a promising way of large-scale production of semiconducting SWCNTs for use in electronics. This has been well studied on isolated SWCNTs, but the implications on the conductivity of SWCNT materials are still unclear. Here, we study the conductivity of such functionalized SWCNT films with a progressively decreased metallic/semiconducting ratio in a wide range of temperatures (4–300 K) to unravel the charge transport mechanisms of metallic and semiconducting SWCNT subnetworks to show how these components participate in the total conductivity of the films. At low functionalization degree (below 0.2 mol%), the conductivity is dominated by a subnetwork of metallic SWCNTs through two parallel mechanisms: a Luttinger liquid mechanism and a Variable Range Hopping process. Higher functionalization (over 0.4 mol%) destroys the Luttinger liquid mechanism, and a second parallel Variable Range Hopping process arises, attributed to the conduction through the semiconducting SWCNTs. At these high functionalization degrees, the SWCNT film behaves as a material with the desired semiconducting properties.

## Graphical abstract

We studied the conductivity of chemically functionalized Single Walled Carbon Nanotube films with a progressively decreased metallic/semiconducting ratio in a wide range of temperatures (4–300 K) to unravel the charge transport mechanisms of metallic and semiconducting SWCNT subnetworks to show how these components participate in the total conductivity of the films.

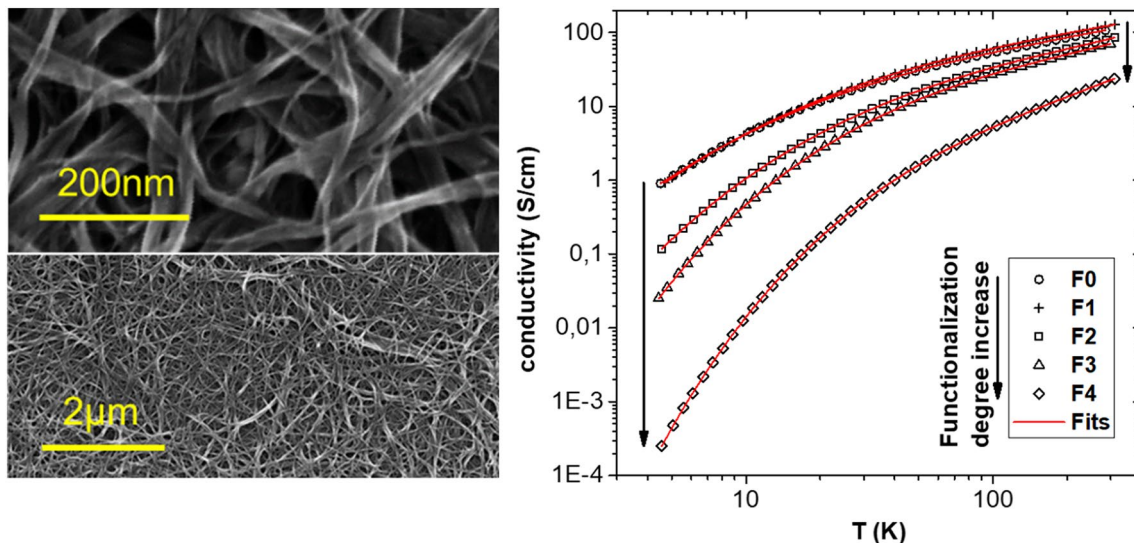
---

**Supplementary Information** The online version contains supplementary material available at <https://doi.org/10.1007/s42452-022-05016-w>.

---

✉ Pascale Chenevier, [pascale.chenevier@cea.fr](mailto:pascale.chenevier@cea.fr); ✉ Jérôme Faure-Vincent, [jerome.faure-vincent@cea.fr](mailto:jerome.faure-vincent@cea.fr) | <sup>1</sup>University of Grenoble Alpes, CEA, CNRS, IRIG, SyMMES, 38000 Grenoble, France. <sup>2</sup>Department of Chemical Physics, Faculty of Chemical and Food Technology, Slovak University of Technology in Bratislava, 81237 Bratislava, Slovakia. <sup>3</sup>University of Grenoble Alpes, CEA, LITEN, DEHT, STB, 38000 Grenoble, France.





**Keywords** Single walled carbon nanotube · Chemical functionalization · Conductivity · Charge transport model · Variable range hopping · Luttinger liquid

## 1 Introduction

Single-wall carbon nanotubes (SWCNTs) have been identified from their discovery as a promising material for electronics. On the one hand, their peculiar electronic structure provides high charge carrier mobility. On the other hand, SWCNTs are also attractive for their low weight, heavy-metal-free composition, and high flexibility, opening ways for new kinds of electronic devices on new substrates such as transparent plastics, stretchable films, papers or textile fibers. In such applications, low cost is an important prerequisite. SWCNTs can meet the needs of low cost fabrication because SWCNT growth cost has considerably dropped with increasing production volume [1, 2], and because very thin SWCNT films provide efficient conductors/semiconductors. Besides, these thin layers can be made by low cost methods such as printing or spraying on plastic [3, 4], paper [5], or rubber [6]. At the research level, electronic circuits based on SWCNTs such as semiconducting transistor channels [7, 8], conductive leads [9], or both [10] have been described with increasing performance in the past 20 years. SWCNTs are also widely used beyond electronics to enhance conductivity in one-dimensional (1D) [11], two-dimensional (2D) [6, 12], and three-dimensional (3D) [13, 14] materials up to commercial development [15].

However, industrial applications of carbon nanotubes as a semiconducting component lag behind. The first reason is that multiwall carbon nanotubes, for which

the development of industrial applications is the most advanced, do not present a real semiconducting gap in their electronic structure, and they are mostly used either as electrical conductors, or in mechanical reinforcement. Only SWCNTs show performant semiconductive behavior. The second reason is that, among SWCNTs, only 2/3 of the chiralities present the semiconducting electronic structure (*sc*-SWCNT) while the other 1/3 has a metallic-type electronic structure (*m*-SWCNT), so that *sc*-SWCNTs have to be separated from *m*-SWCNTs, that would entail short-circuits, to take advantage of their excellent semi-conductive performance. Recent advances towards applications have been made possible by intensive research on the separation of SWCNTs in metallic and semiconducting pure species. Smart polymers designed to show a specific affinity for a single chirality of SWCNT allow for specific dissolution of this single chirality in organic solvents [16, 17]. Another separation method relies on aqueous polymer biphasic systems using the slight hydrophobicity difference between SWCNT chiralities [18]. Those methods allow for the preparation of solutions of individual *sc*-SWCNT species [19], that found astounding applications in plastic electronics [7], solar cells [20], light emission [21] or optics [22]. However, such high selectivity separation can only be obtained with high cost polymers and/or iterative separation steps, resulting in very dilute and high price *sc*-SWCNT solutions. High throughput fabrication of printed electronics requires larger scale and

lower cost semiconducting materials, and should be less demanding towards conductivity and purity targets. Besides, other bulk-material-based applications would benefit from *sc*-SWCNTs at large scale, such as thermoelectric generators [23] and devices, for which doped SWCNTs [24] and SWCNT-polymer composites [25] show a high efficiency.

Alternatively, we proposed a non-separative method to tune the semiconducting behavior of a native *m*-/*sc*-SWCNT mixture by using diazo coupling on SWCNTs in aqueous solution [26, 27]. This method takes advantage of the difference in SWCNT chemical reactivity as a function of chirality, *m*-SWCNTs being more reactive than *sc*-SWCNTs towards covalent functionalization with diazo reagents. As covalent bonds disrupt the local electronic structure of the SWCNT [28], a high level of functionalization reduces its electrical conductivity. The diazo reagent and the reaction conditions were engineered to enhance as much as a factor of 100 the reaction rate on *m*-SWCNT compared to *sc*-SWCNT, so that all accessible *m*-SWCNTs can be functionalized selectively. The resulting unseparated material provides a proper semiconducting material, as we showed previously for field-effect transistor (FET) channels [4]: compared to pristine SWCNTs FETs, optimized functionalized SWCNT FETs show improved performances (increase of the  $I_{on}/I_{off}$  ratio by 500) whereas the mobility remains similar.

Studies on diazo coupling to SWCNT give a quite accurate picture of the chemical structure of the material at the molecular level [26, 28–32]. The impact of covalent functionalization on the electronic structure of individual SWCNTs has been experimentally measured operando [33, 34] and their mesoscopic conductance modelled by numerical simulations [35]. Besides, the contact resistance of carbon nanotube crossings was investigated in single interconnections [36–40].

Yet for potential electronic applications of functionalized SWCNTs, it is the behavior of macroscopic materials that is crucial. It is important to know to what extent the charge transport in these materials has the desired semiconducting properties. The percolation behavior in films of *m*- and *sc*-SWCNT at room temperature was the subject of numerous experimental and numerical studies [41, 42] from this point of view. A powerful tool to determine the charge transport mechanism in materials is the study of the temperature dependence of their conductivity, since different mechanisms induce distinct characteristic features. The impact of different *m*/*sc* SWCNT concentrations on the conductivity temperature dependence  $\sigma(T)$  of the resulting material has been studied in a few papers which varied the *m*/*sc* ratio by mixing sorted *m*- and *sc*-SWCNTs species [43–46]. These

results mostly found that the electronic transport in *sc*-SWCNT unaligned networks is dominated by hopping.

In spite of the progress made by these works, it is still not clear how the *m*- and *sc*-components participate in the total conductivity in functionalized native mixtures when the *m*/*sc* ratio is progressively decreased by chemical modification and at which value of this ratio the material can be considered semiconducting. A possible approach to solve this problem is to study the conductivity mechanisms of progressively diazo functionalized pristine SWCNTs. The present work relies on low temperature  $\sigma(T)$  measurements coupled to conductivity mechanism modelling to enlighten the underlying conductivity mechanisms in SWCNT films as a function of the functionalization degree. Since different mechanisms are expected for *m*- and *sc*-SWCNTs, their relative weight evolution enables to identify and to quantify the *m*- and *sc*-SWCNTs contributions to the total  $\sigma(T)$  for different chemical functionalization degrees and thus to describe the progressive transformation of the *m*/*sc* mixture to a material with the requested semiconducting properties.

## 2 Experimental methods

### 2.1 SWCNTs film preparation

SWCNTs (arc discharge) were functionalized by reaction with the nitrophenyldiazoether of ascorbic acid, the most selective reagent towards *m*-SWCNTs, following the processes established in our previous work [4, 27]. The diazoether was added to SWCNTs dispersed in water with a cationic surfactant, and then rinsed before spraying. We chose 4 different diazoether/SWCNT molar ratios from 1.8 to 22% (labeled F1 to F4 in Fig. 1) to span the range from low to high SWCNT functionalization yield.

More precisely, pristine SWCNTs (Carbon Solutions Inc.) were dispersed (5 g/L) in an aqueous solution of hexadecyltrimethylammonium bromide (CTAB, 0.2%) by sonication, and centrifuged (60,000g, 20 h). The 20% bottom part, where the agglomerated SWCNTs concentrate, was removed, and the top solution was diluted to a final concentration of 0.2 g/L and buffered to pH 1 by adding phosphoric acid (100 mM). This SWCNT solution was treated with diazoether as follows: 4-nitrobenzenediazonium tetrafluoroborate (0.4 mmol) and ascorbic acid (0.44 mmol) were dissolved in cold water (20 mL) and incubated for 1 min to allow for the formation of diazoether. To 100 mL of SWCNT solution was added 1.12 mL, 2.25 mL, 4.5 mL, 13.5 mL, and 0 mL of diazoether solution to prepare samples, labeled F1, F2, F3, F4 and F0, respectively. After 30 min of reaction, the SWCNTs were precipitated by adding 100 mL ethanol, filtered and washed with ethanol,



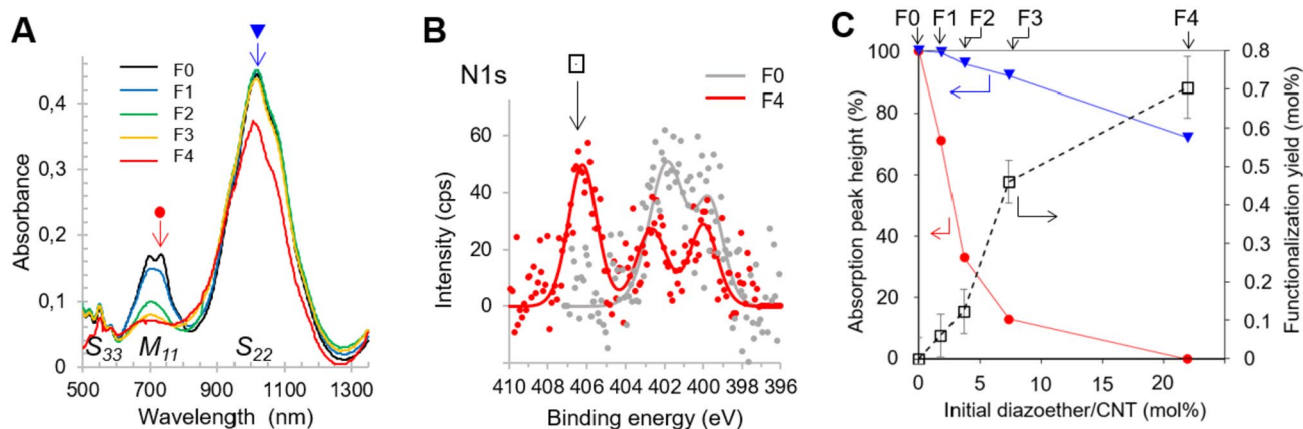


**Fig. 1** Characterization of SWCNT samples as a function of functionalization degree. A: Background-subtracted absorption spectra of the SWCNTs in solution, showing the van Hove peaks of the  $S_{22}$  transition at 1050 nm (triangle, *sc*-SWCNTs) and of the  $M_{11}$  transition at 730 nm (dot, *m*-SWCNTs). B: N1s XPS spectra of pristine (grey) and functionalized (red) SWCNTs, showing the  $NO_2$

peak (pointed by a square) at 406.5 eV: experimental data (dots), and Gaussian fit (line). C: Changes in SWCNT absorption peaks at 1050 nm (triangles) and 730 nm (dots), and in  $NO_2$  peak (functionalization yield) by XPS (squares) as a function of functionalization extent (initial diazoether/CNT ratio). Labels above the graph define the corresponding samples

and dispersed in CTAB 0.2% solution. The final SWCNT concentration was adjusted to 80 mg/L for spray.

The polyethylene naphthalate (PEN) substrate was first treated by  $O_2$  plasma for a better adhesion of SWCNTs. The substrate was spray-coated at 80 °C with the SWCNT aqueous dispersion (120 kHz ultrasonic ExaTaCoat spray coater) through a shadow mask (0.25 ml/min throughput, 50 mm/s path speed to reduce coffee ring effect). The substrate was dipped into slightly warm (60 °C) water for 5 s and rinsed with isopropanol to remove CTAB after each deposition. The spray deposition was repeated several times to obtain an approx. 45 nm-thick film of unaligned SWCNTs (thickness within 12% error, see Table S1), as measured by its light absorption (Absorbance = 0.16 at a wavelength of 800 nm, Fig. 2c). Choosing approx. 45 nm as the thickness for all samples allows conductivity

measurements down to a temperature of 4 K even for the most resistive (highly functionalized) samples. This ensures a good quality of conductivity measurement and a wide enough range of temperatures for a proper transport model interpretation. The transmittance at 550 nm of the SWCNT films is available in table S1 (see Supplementary Material).

### 2.2 Temperature dependence of dc conductivity

To perform the temperature dependence of dc conductivity measurements, rectangular samples (length and width approx. 15 and 4 mm, respectively) were cut from the prepared samples. To ensure proper electrical measurements, gold contacts (200 nm-thick) were deposited on the samples by using a shadow mask. The electrical measurements

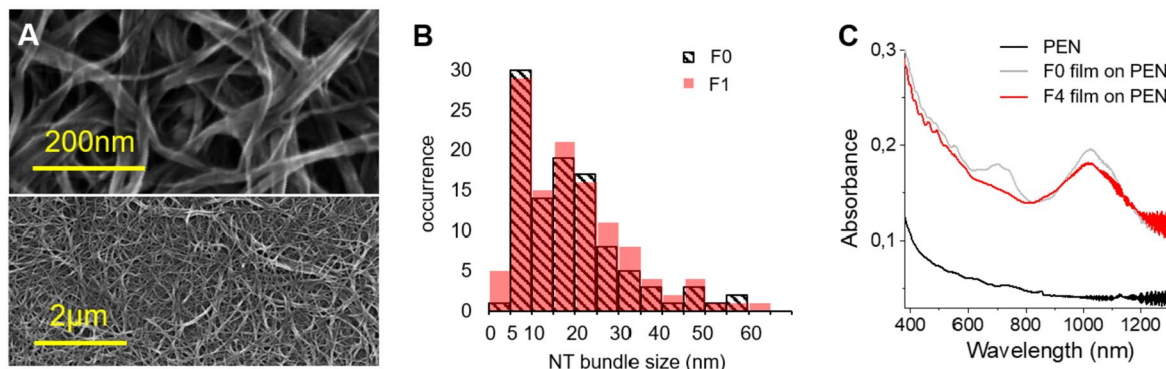


**Fig. 2** SWCNT films by spray. A: Scanning electron microscopy (SEM) images of SWCNT films prepared by spray on PEN. B: size histogram of SWCNT bundles in the film from SEM images. C: Absorption spectra of SWCNT films

were performed using the standard four-probe method by a combination of a Keithley 220 current source and Keithley 6512 electrometer. The distance between the inner probes was 2.9 mm. The temperature varied from 4 K up to 300 K using a dynamic helium flow cryostat Oxford Instruments CF 1200 D. To limit the sample heating during the measurement, we paid attention to keep the injected electrical current as low as possible while high enough to get a clear voltage drop (typically a few mV). Thus, the dissipated power was kept below a few hundreds of nWs. In addition, a helium atmosphere with the requested temperature surrounded the sample. This ensured an efficient sample temperature stabilization thanks to He thermal convection. At each measurement, the ohmic character of the resistance was checked. The sheet resistance of the SWCNT films at room temperature is available in table S1 (see Supplementary Material).

### 3 Results and discussion

#### 3.1 Functionalization of SWCNT by nitrophenyldiazoether

The absorption spectra of the SWCNT suspensions (Fig. 1a) show the extent of functionalization for the 5 samples F0–F4: the typical van Hove absorption peak of *m*-SWCNTs at 690–740 nm (circle) is continuously reduced along the functionalization. This corresponds to the destruction of the delocalized electron structure of the SWCNTs due to the addition of covalent bonds between the carbons of the SWCNTs and the nitrophenyl moieties. Thanks to the high

selectivity of the chosen diazoether towards *m*-SWCNTs, the *sc*-SWCNTs are much less functionalized, as observed by the low decrease of the corresponding van Hove peak at 900–1140 nm (triangle). The functionalization yield could also be measured by XPS (Fig. 1b): the NO<sub>2</sub> moiety of nitrophenyl gives a specific signal in the N1s spectrum at 406 eV (square). As described in our previous studies [4, 27, 28], this signal rises continuously with the extent of functionalization, in accordance with the absorption spectroscopy data (Fig. 1c).

When drying on the surface during the spray deposition, the SWCNT bundles are arranged in SWCNT ropes (Fig. 2a), building an entangled network of highways for electronic transport. These highways are much thinner (5–30 nm, Fig. 2) than the typical distance between two interlope contacts (~ 100 nm).

#### 3.2 Conductivity of SWCNT films

Figure 3 shows the measured  $\sigma(T)$  curves. The temperature interval was 4–300 K. The analysis over such a large temperature range (two orders of magnitude) allows for discriminating between the different transport models. In addition, only few studies focus on the conductivity of SWCNT materials at temperatures below 10 K, which is of primary importance to study the behavior when  $T \rightarrow 0$  K. To highlight more clearly the limiting 0 K behavior, we represent our data in double logarithmic scales (Fig. 3a) (the fits associated with these results will be discussed later). All curves are monotonically increasing concave functions of temperature, clearly showing a zero conductivity at  $T=0$  K limit. Their absolute values decrease with increasing

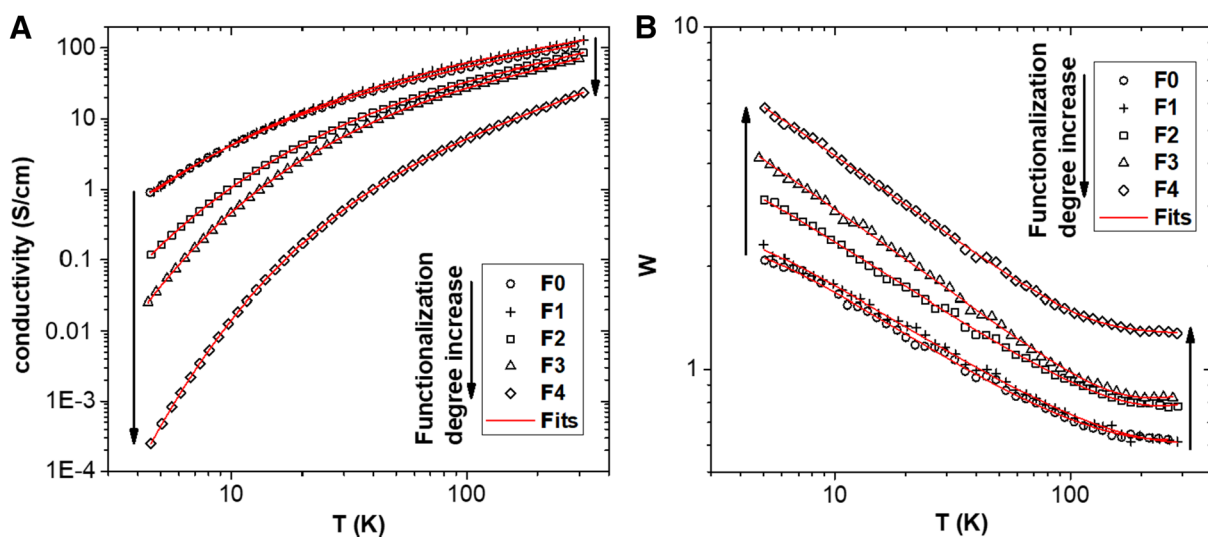


**Fig. 3** Conductivity  $\sigma$  (A) and reduced activation energy  $W$  (B) as a function of temperature for different functionalization degrees. Continuous lines show the best fits

functionalization degree mainly at low temperatures as plotted in Fig. 3a. Monotonically increasing  $\sigma(T)$  in SWCNT-based materials were mainly explained by the following general electronic transport mechanisms (see e.g. [47–49] and references therein): the Fluctuation Induced Tunneling, the Weak Localization model, the Critical Regime of the Metal–Insulator Transition (MIT), the Luttinger Liquid, the Simple Thermally Activated Behavior and the Variable Range Hopping. They cover a wide range of  $\sigma(T)$  regimes from the “metallic regime” on the metallic side of the MIT where, by definition,  $\lim_{T \rightarrow 0} \sigma(T) \neq 0$ , to the “insulating regime” on the insulating side of the MIT where, by definition,  $\lim_{T \rightarrow 0} \sigma(T) = 0$ .

- (i) The Fluctuation Induced Tunneling (FIT), also known as Sheng’s model [50], describes the conductance between two 3D metallic regions separated by thin barriers when temperature-activated voltage fluctuations across the insulating barrier are taken into account. The conductivity is expressed as

$$\sigma = \sigma_0 \exp\left[\frac{-T_b}{T + T_s}\right] \tag{1}$$

where  $\sigma_0$  is a constant prefactor,  $T_b$  and  $T_s$  are characteristic temperatures.

- (ii) The Weak Localization (WL) model takes into account the electron–electron interactions in weakly disordered metals on the metallic side of the MIT in the frame of the Anderson model [51]. Weak Localization originates from the quantum interference of time-reversed paths in electron transport [49]. At low temperatures, the conductivity follows

$$\sigma = \sigma_0 + mT^{1/2} \tag{2}$$

where  $\sigma_0$  and  $m$  are constants.

- (iii) The Critical Regime corresponds to the transition between the metallic and insulating regimes of  $\sigma(T)$ . In the frame of the Anderson model, the Critical Regime occurs when the electron mean free path is smaller than the correlation length. Then the conductance follows a power law  $G \propto T^\beta$  with  $\beta$  between 1/3 and 1 [52].
- (iv) A Luttinger Liquid (LL) refers to a correlated ground state in a 1D metal [53]. The transport through tunnel junctions into and out of a Luttinger Liquid, as well as through a tunnel junction connecting two Luttinger liquids, is expressed by a power law,  $G \propto T^\alpha$ . Metallic SWCNTs are 1D conductors and thus can be considered as LLs. One defect on a SWCNT divides the SWCNT into two Luttinger Liquids

separated by a thin tunnel barrier. In this case, the exponent  $\alpha$  depends on the Luttinger parameter  $g$  describing the influence of the Coulomb interactions [54, 55] as

$$\alpha = \frac{(g^{-1} - 1)}{2} \tag{3}$$

The charge transport in the insulating regime of  $\sigma(T)$  is mostly described by the two following mechanisms.

- (v) The Simple Thermally Activated Behavior [56] is expressed by the formula

$$\sigma = \sigma_0 \exp\left(\frac{-E_a}{k_B T}\right) \tag{4}$$

where  $\sigma_0$  is a constant prefactor,  $E_a$  is the activation energy of the charge transport, and  $k_B$  is the Boltzmann constant.

- (vi) The Variable Range Hopping (VRH), also known as Mott model, corresponds to a charge transport driven by phonon-assisted tunneling between localized states in disordered materials [57]. The VRH theory describes the transport between localized states close to the Fermi level in a disordered structure. The conductivity is approximately described as

$$\sigma = \sigma_0 \exp\left[-\left(\frac{T_0}{T}\right)^n\right] \tag{5}$$

where  $\sigma_0$  is a constant,  $T_0$  is a parameter and the exponent  $n$  can be expressed as  $n = 1/(d+1)$ , where  $d$  is the dimensionality of the transport ( $n = 1/2, 1/3$  or  $1/4$  corresponds to 1D, 2D or 3D transport, respectively). The parameter  $T_0$  depends on the density of states at the Fermi level  $N(E_F)$  and on the charge localization length  $\xi$  in the disordered material following the relation

$$T_0 \propto \frac{1}{\xi^d N(E_F) k_B}, \tag{6}$$

with  $k_B$ , the Boltzmann constant. When the Coulomb interactions are taken into account in the 3D case of the VRH transport, then  $n = 1/2$  instead of  $1/4$  (Efros-Shklovskii model) [58].

Since our samples are disordered and undoped thin films of small bundles of SWCNTs, it is highly probable that they are on the insulating side of the MIT [49]. This means that the Sheng’s and the Weak Localization models, which are on the metallic side of the MIT, can be eliminated as involved transport mechanisms.

Regarding the remaining mechanisms (featuring zero conductivity at the zero temperature limit), we note that, from the strict mathematical point of view, Eq. 4 is formally equivalent to Eq. 5 if  $n = 1$  and similarly, the power law equations corresponding to the Luttinger Liquid and Critical Regime are formally equivalent. Thus, we are left with only two types of mathematical expressions to fit our results: the VRH-type and the power law.

The conductivity can be further analyzed in the form of the reduced activation energy [59]  $W$ , defined as

$$W(T) = \frac{d \ln \sigma(T)}{d \ln T} = T \frac{d \ln \sigma}{dT}. \quad (7)$$

The study of  $W(T)$  proved to be a powerful tool to analyze the transport mechanisms and the MIT in several organic materials such as conductive polymers [60, 61], in carbon nanotubes [49, 62–65] or in carbon nanotube/polymer composites [66]. As a derivative,  $W(T)$  is more sensitive than  $\sigma(T)$  to hidden transport mechanisms. Besides, using  $W(T)$  lowers the number of fitting parameters by eliminating the constant prefactor of  $\sigma(T)$ , thus making the fitting more reliable. Therefore, we first analyzed our  $W(T)$  data (Fig. 3b) instead of  $\sigma(T)$  (Fig. 3a).

In general, at  $T \rightarrow 0$ , near the MIT,  $W(T)$  is an increasing function of temperature in the metallic regime, a constant function exactly at the MIT (critical regime, power-law  $\sigma(T)$ ) and a decreasing function of temperature in the insulating regime [59, 60].

In our case, all  $W(T)$  curves (Fig. 3b) are decreasing functions of  $T$  as expected from Fig. 3a. Since on the metallic side of the MIT the reduced activation energy  $W$  should be an increasing function of  $T$ , this justifies our choice not to consider the WL or FIT, which belong to the mechanisms describing  $\sigma(T)$  in the metallic regime, as possible models in our analysis, at least as a single mechanism or associated in parallel with any other mechanism.

The strongest feature of Fig. 3b is an almost linear behavior at temperatures below 100 K, which is typical of a VRH mechanism for which  $\log(W) = \text{constant} - n \log(T)$  (following Eq. 5). It shows that a VRH mechanism clearly prevails in our samples at low temperatures. This observation is in agreement with the results on undoped SWCNT films for any  $m/sc$  ratio obtained by Yanagi et al. [43], Bulmer et al. [44] and Wang et al. [46], and in contradiction with those of Itkis et al. [45] who fitted their low-temperature conductivity experiments by the FIT mechanism. If we limited the temperature range of the analysis below 100 K, as done, e.g., by Yanagi et al. [43], we would obtain interpretation of the material electronic conductivity with decreasing  $m$ -SWCNT content in terms of the parameters evolution of only one VRH-type transport

mechanism. Nevertheless, all curves deviate from the linear regime at high temperature (over 100 K) where  $W(T)$  flattens. In addition to the high temperature flattening, the two less functionalized samples (F0 and F1) slightly deviate from the linear regime also at low temperature (see Figure S1). It implies that an additional mechanism is associated with the above-cited VRH-type mechanism. The need for combining two transport mechanisms to account for the conductivity from low to room temperature was often recognized [45, 47, 48].

In real disordered materials, a combination of two mechanisms corresponds to a complicated series-parallel circuit. To analyze such circuits, a simplification is necessary by considering a simple series or parallel circuit. Such a physical approach has already been successfully used [45, 47, 48, 66] on carbon-nanotube-based systems. VRH-type and power law were recognized as the only possible mathematical functions in our case. Consequently, we analyzed our  $W(T)$  data by studying the “VRH-VRH” and “VRH-power law” combinations (in series or in parallel). We observed that the combination in series did not lead to satisfactory fits whatever the functionalization degree. On the contrary, we found that only a “VRH-power law” parallel combination led to excellent fits over the whole temperature range for samples F0, F1, and F2, while for F3 and F4 samples, only a “VRH-VRH” parallel combination led to excellent fits over the whole temperature range.

As a result, for F0, F1, and F2, the fitting functions of  $\sigma(T)$  can be written as the sum of a VRH-conductivity  $\text{VRH}_1$  (noted  $\sigma_1$ ) and of a power law conductivity (noted  $\sigma_2$ ),

$$\sigma(T) = \sigma_1(T) + \sigma_2(T) = \sigma_{01} \exp \left[ - \left( \frac{T_{01}}{T} \right)^{n_1} \right] + \sigma_{02} T^\alpha \quad (8)$$

(5 fitting parameters  $\sigma_{01}$ ,  $n_1$ ,  $T_{01}$ ,  $\sigma_{02}$ ,  $\alpha$ ) and  $W(T)$  can be written as

$$W(T) = \frac{n_1 \left( \frac{T_{01}}{T} \right)^{n_1} \exp \left[ - \left( \frac{T_{01}}{T} \right)^{n_1} \right] + \alpha \frac{\sigma_{02}}{\sigma_{01}} T^\alpha}{\exp \left[ - \left( \frac{T_{01}}{T} \right)^{n_1} \right] + \frac{\sigma_{02}}{\sigma_{01}} T^\alpha} \quad (9)$$

(4 fitting parameters  $n_1$ ,  $T_{01}$ ,  $\alpha$ ,  $\sigma_{02}/\sigma_{01}$ ).

For F3 and F4, the fitting functions of  $\sigma(T)$  can be written as the sum of a VRH-conductivity  $\text{VRH}_1$  (noted  $\sigma_1$ ) and another VRH-conductivity  $\text{VRH}_3$  (noted  $\sigma_3$ ),

$$\sigma(T) = \sigma_1(T) + \sigma_3(T) = \sigma_{01} \exp \left[ - \left( \frac{T_{01}}{T} \right)^{n_1} \right] + \sigma_{03} \exp \left[ - \left( \frac{T_{03}}{T} \right)^{n_3} \right] \quad (10)$$

(6 fitting parameters  $\sigma_{01}$ ,  $n_1$ ,  $T_{01}$ ,  $\sigma_{03}$ ,  $n_3$ ,  $T_{03}$ ) and  $W(T)$  can be expressed as



$$W(T) = \frac{n_1 \left(\frac{T_{01}}{T}\right)^{n_1} \exp\left[-\left(\frac{T_{01}}{T}\right)^{n_1}\right] + n_3 \frac{\sigma_{03}}{\sigma_{01}} \left(\frac{T_{03}}{T}\right)^{n_3} \exp\left[-\left(\frac{T_{03}}{T}\right)^{n_3}\right]}{\exp\left[-\left(\frac{T_{01}}{T}\right)^{n_1}\right] + \frac{\sigma_{03}}{\sigma_{01}} \exp\left[-\left(\frac{T_{03}}{T}\right)^{n_3}\right]} \tag{11}$$

(5 fitting parameters  $n_1, T_{01}, n_3, T_{03}, \sigma_{03}/\sigma_{01}$ ).

In these equations,  $\sigma_{01}, \sigma_{02}$ , and  $\sigma_{03}$  are the prefactors of the partial conductivities  $\sigma_1, \sigma_2$ , and  $\sigma_3$ , respectively,  $T_{01}$  and  $T_{03}$  are the characteristic parameters (with the physical dimension of temperature) of  $\sigma_1$  and  $\sigma_3$ , respectively,  $n_1, \alpha$ , and  $n_3$  are the exponents of  $\sigma_1, \sigma_2$  and  $\sigma_3$ , respectively.

### 3.3 Resulting fit parameters

We first used the Eqs. 9 and 11, which have less fitting parameters and therefore lead to more reliable fits, to fit the  $\log W$  vs  $\log T$  data (see Fig. 3b). The parameters  $n_1, T_{01}, \alpha, n_3, T_{03}$  presented in Table 1 were obtained from these fits. Subsequently, using these parameters, the  $\log(\sigma)$  vs  $\log(T)$  data (see Fig. 3a) are fitted by using the Eqs. 8 and 10 to get the prefactor values ( $\sigma_{01}, \sigma_{02}$  and  $\sigma_{03}$ ) driving the partial conductivities. Both the  $W(T)$  and  $\sigma(T)$  fits show excellent agreement over the whole temperature range for all samples (Fig. 3a, b).

The values of the parameters in Table 1 lead to the following conclusions.

First, one Variable Range Hopping component (labeled  $VRH_1$ , with an exponent  $n_1$  close to 0.5) is present for all samples. This exponent is consistent with a 1D transport mechanism in such a 1D-material as individual SWCNTs. However, we cannot exclude a 3D VRH in the frame of the Efros-Shklovskii [58] model which takes into account the Coulomb interactions. Such a situation might correspond to a 3D electronic transport between SWCNTs within a bundle or from bundle to bundle, as found by [44]. This  $VRH_1$  mechanism shows a parameter  $T_{01}$  close to room temperature at low functionalization, raising when the functionalization increases. Similar values have been reported for VRH in SWCNT films [46] or were foreseen by simulation for chemically functionalized SWCNTs [67], and correspond to a transport with low thermal activation.

Second, for the power law  $T^\alpha$  (Eqs. 8 and 9) observed in the samples F0, F1, F2, exponents  $\alpha$  between 1.18 and 1.9 were found (see Table 1). Such a power law cannot be attributed to a Critical Regime for which the exponent cannot be superior to 1 [52]. Therefore, we associate this power law function to the signature of a Luttinger Liquid mechanism in a 1D metal (metallic nanotubes). The optical absorption data in Fig. 1c showing an important presence of  $m$ -SWCNTs in the samples F0, F1, and F2, support this interpretation. Extracting the Luttinger parameter  $g$  from the fitted  $\alpha$  values according to Eq. 3, we obtain  $g = 0.30, 0.29$ , and  $0.21$  for the samples F0, F1, and F2, respectively. The two first values are in good agreement with the theoretical estimate  $g \approx 0.28$  [53, 68, 69]. The third value ( $g = 0.21$ ) differs slightly from this theoretical value but is close to the experimental value 0.22 reported in the literature as corresponding to a barrier (kink shaped defect) between two metallic sections of a SWCNT [54]. We note that Bulmer et al. [44] observed a power-law  $\sigma(T)$  with  $\alpha = 0.2$  in a film of unsorted SWCNTs (i.e. approximately comparable to our sample F0), and with  $\alpha = 0.36$  in a film of containing 95% of  $m$ -SWCNTs, but only after nitric acid doping so that it is not possible to simply compare their results with the power-law  $\sigma(T)$  component observed in our experiment.

Third, for the parameters of the Variable Range Hopping  $VRH_3$  component appearing in the F3 and F4 samples, the direct fits involving two VRH formulae (i.e., two similar mathematical functions) are unfortunately not sensitive enough to determine  $n_3$ . Values of  $n_3$  from 0.25 to 0.5 were tried as fitting parameters. Fits with  $n_3 = 0.25$  lead to extremely high  $T_{03}$  values ( $> 10^6$  K), see Table S2, and thus to a negligible density of states for the corresponding transport mechanism (see Eq. 6). Therefore, a fixed value of  $n_3 = 0.5$  was used for the fit, leading to  $T_{03}$  values around 8000 K, indicative of a much more hindered transport mechanism for  $VRH_3$  than for  $VRH_1$ .

Figures 4a, b illustrate the absolute contribution and Fig. 4c, d the relative contribution (in logarithmic scale) of the partial conductivities  $\sigma_1, \sigma_2$ , and  $\sigma_3$  to the total conductivity  $\sigma$  (Eqs. 8 and 10) as a function of the

**Table 1** Fitting parameters obtained from the fits using Eqs. 8, 9, 10, and 11

Sample	VRH <sub>1</sub> component			Power law (Luttinger Liquid) component		VRH <sub>3</sub> component		
	$\sigma_{01}$ (S/cm)	$n_1$	$T_{01}$ (K)	$\sigma_{02}$ ((mS/cm)/K <sup><math>\alpha</math></sup> )	$\alpha$	$\sigma_{03}$ (S/cm)	$n_3$ (fixed)	$T_{03}$ (K)
F0	1700 ± 200	0.45 ± 0.01	200 ± 20	40 ± 5	1.18 ± 0.03	0	NA	NA
F1	2500 ± 200	0.43 ± 0.01	270 ± 30	26 ± 2	1.23 ± 0.05	0	NA	NA
F2	2200 ± 200	0.44 ± 0.01	460 ± 60	0.40 ± 0.05	1.9 ± 0.2	0	NA	NA
F3	2000 ± 200	0.49 ± 0.01	400 ± 20	0	NA	2000 ± 200	0.5	9000 ± 1000
F4	1000 ± 100	0.48 ± 0.01	960 ± 40	0	NA	1000 ± 100	0.5	7800 ± 500

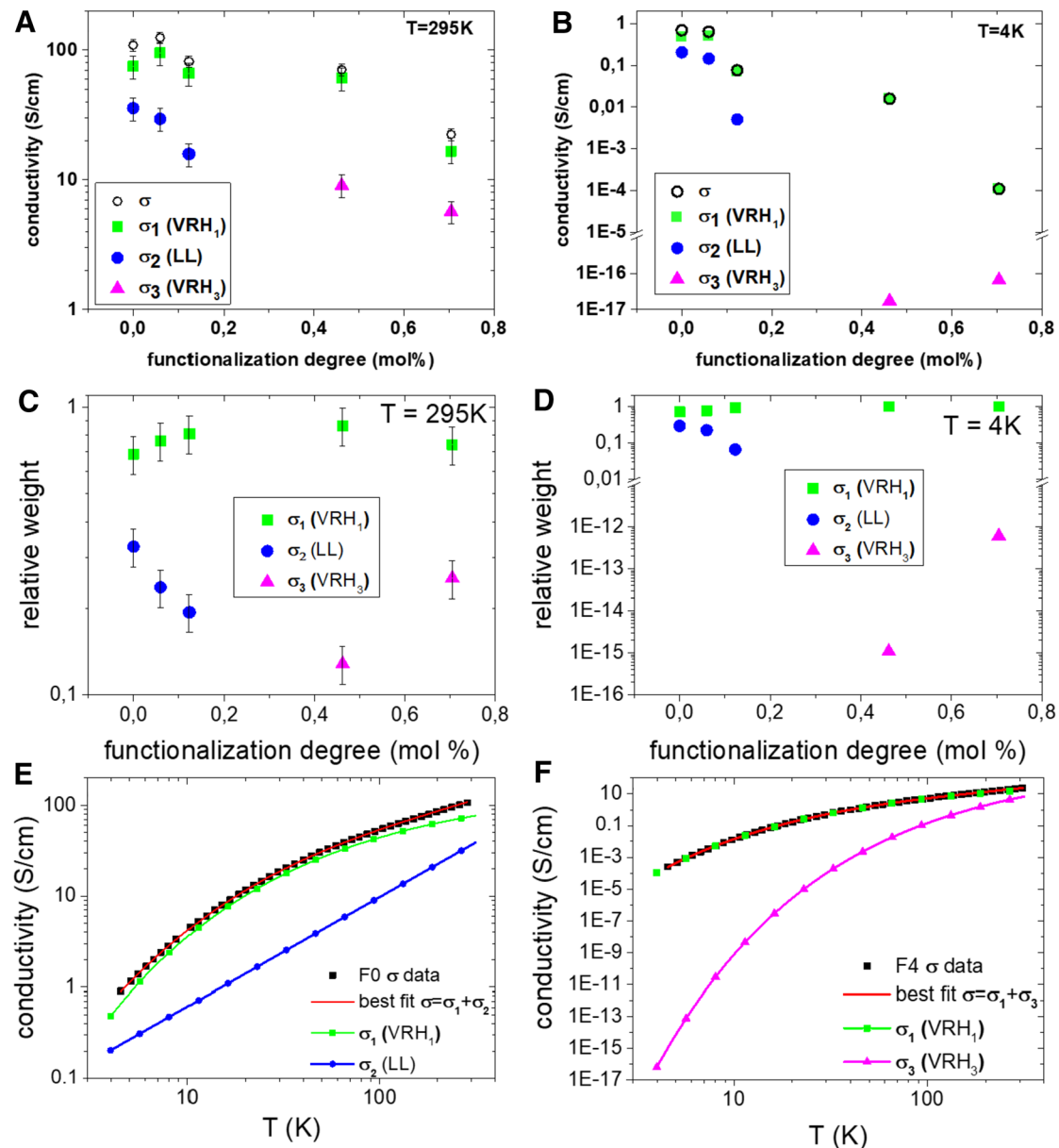


**Fig. 4** Total ( $\sigma$ ) and partial ( $\sigma_1$ ,  $\sigma_2$ ,  $\sigma_3$ ) conductivities (in logarithmic scale) as a function of the functionalization degree for T=295 K (A) and T=4 K (B); weight of the partial conductivities in the total conductivity at 295 K (C) and at 4 K (D). Exam-

ple of decomposition of the total conductivity  $\sigma$  as a function of temperature into components with different transport mechanisms for the samples F0 (E) and F4 (F). For (B) and (D), the error bars are smaller than the point size

functionalization degree at  $T=295$  K and  $T=4$  K, respectively. Figure 4e, f illustrate the decomposition of the total conductivity  $\sigma(T)$  along  $\sigma_1(T)$ ,  $\sigma_2(T)$ , and  $\sigma_3(T)$  as a function of temperature for the extreme F0 and F4 samples, respectively.

At room temperature ( $T=295$  K, Fig. 4a), starting from F1, the total conductivity and the component  $\sigma_1$ , as well as the two remaining components  $\sigma_2$  and  $\sigma_3$  (in the case where they are not zero), decrease with the functionalization degree. The contribution of the  $\sigma_2$  part disappears

and is replaced by the  $\sigma_3$  component between 0.12 and 0.46 mol% functionalization.

At 4 K (Fig. 4b), the situation is similar, except that here the  $\sigma_3$  contribution increases with the functionalization degree but still remains negligible, as expected at low temperatures from the very high parameter  $T_{03}$ .

The relative weights of the partial conductivities in the total conductivity at 295 K and 4 K are shown in Fig. 4c, d, respectively. At both temperatures, the total conductivity is dominated by  $\sigma_1$  (roughly between 70 and 90% at

295 K and between 70 and 100% at 4 K) and the  $\sigma_3$  relative weight increases with the functionalization degree.

Figure 4e, f show that the above-described behaviors are valid for any measured temperature.

## 4 Discussion

Figure 4 thus leads to the conclusion that the functionalization progressively transforms the SWCNT film from a material with a relatively high total conductivity composed of two parallel mechanisms VRH<sub>1</sub> and LL to a genuinely fully semiconducting material with a lower total conductivity composed of two parallel mechanisms VRH<sub>1</sub> and VRH<sub>3</sub>. The presence and progressive transformation of the conductivity mechanisms with increasing functionalization degree can be explained as follows.

### 4.1 Metallic SWCNTs

From the electronic point of view, a defect on the *m*-SWCNT corresponds to a tunnel barrier separating two metallic sections of SWCNT. One defect thus creates a situation equivalent to two Luttinger Liquids connected end-to-end by a tunnel barrier. The high values of  $\alpha$  ( $\alpha > 1$ , see Table 1) are typical of end-to-end connected LLs [54] and support this interpretation. In this picture, more degraded *m*-SWCNTs (i.e., with two or more defects) are cut into shorter metallic sections. These sections can be viewed as localized states between which the transport is realized by hopping, a typical semiconducting behavior. The observed VRH<sub>1</sub> transport can be attributed to this mechanism. Thus, within the material, the *m*-SWCNTs contribute to the total electronic transport by two parallel mechanisms (taking place in two percolating subnetworks): the LL mechanism ( $\sigma_2$ ) in long metallic sections of SWCNTs separated by thin tunnel barriers, and the ‘semiconducting-like’ VRH ( $\sigma_1$ ).

These two mechanisms coexist already in non-functionalized samples because of the presence of intrinsic defects on the *m*-SWCNTs. The functionalization creates additional barriers on the *m*-SWCNTs and breaks them into shorter metallic sections with random lengths. This leads to an increased number of LL resistances in series and therefore to a strong decrease of the resulting  $\sigma_2$  conductivity (Fig. 4a, b), and of the total conductivity of the sample (Fig. 3a). In the case of high functionalization, the LL percolating subnetwork completely disappears, and electrical transport through the *m*-SWCNTs is only possible through the VRH<sub>1</sub> hopping mechanism. Shorter metallic sections also mean smaller localization lengths [57] of the electronic states ( $\xi$ ) within the frame of VRH<sub>1</sub>. This is in agreement (Eq. 2) with the observed increase of the

parameter  $T_{01}$  from 200 to 900 K (Table 1) with increasing functionalization degree.

### 4.2 Semiconducting SWCNTs

Strong functionalization of the material affects not only *m*-SWCNTs but, at a lower degree, also *sc*-SWCNTs, as shown in Fig. 1 and in our previous works [4, 26–28]. In *sc*-SWCNTs, the creation of random defects leads to a disordered material with localized states in the bandgap of the originally non-functionalized *sc*-SWCNTs. The creation of the mid-gap states increasing the conductivity in *sc*-SWCNTs by functionalization was evidenced in single SWCNT studies by Bouilly et al. [34]. An additional Variable Range Hopping, VRH<sub>3</sub>, can thus occur between the created localized states near the Fermi level. These localized states are rare (low  $N(E_F)$ ), in agreement with the much higher parameter  $T_{03}$  compared to  $T_{01}$  (see Eq. 6). In our analysis, this low-conduction channel appears as  $\sigma_3$  in Fig. 4. Thus, the functionalization induces an additional transport mechanism through the *sc*-SWCNTs.

In our analysis, we didn’t explicitly consider inter-nanotube contact resistance which is known to play a role in the total conductance of SWCNT-networks [70, 71]. There are three types of inter-nanotube contact resistances to take into account: *m*-*m*, *m*-*sc* and *sc*-*sc*. In the case of a *m*-*m* contact between two LLs, if the contact resistance is higher than the LL resistance of the *m*-SWCNTs, it simply eliminates the connected parts from the LL subnetwork and thus does not appear in the resulting LL conductivity of the network. In all other cases (*m*-*m* where at least one of the nanotubes is in the VRH<sub>1</sub> regime, *m*-*sc* and *sc*-*sc*), the contacts may be considered as additional potential barriers between localized states in the frame of the VRH mechanism and at least some of them may be included into the VRH. Since an extremely broad statistical distribution of the contact resistances is usually observed in the SWCNT networks [71], additional either very high or negligible resistances are probably present in the network but have no impact on the transport mechanisms because they either eliminate one part of the subnetwork or do not affect the subnetwork from the resistance point of view, respectively.

We note that in the absorbance spectra, a small *m*-SWCNT absorbance band remains even for highly functionalized samples. This is because SWCNTs are prepared as a suspension of small bundles [4] containing from a few tubes up to a few tens of tubes, in the core of which a small fraction of the SWCNTs are inaccessible to functionalization. Complete separation of SWCNTs in solution is possible, but requires a longer purification, with a much lower yield. From the spectroscopy records, the part of non-functionalized *m*-SWCNTs in the highly functionalized

samples can be estimated to be < 5%. However, from the electronic transport point of view, the contribution of the LL component, related to the presence of long metallic sections of *m*-SWCNT, disappears at high functionalization degree (see Fig. 4). Thus, some non-functionalized *m*-SWCNTs are still present, but they do not contribute to the conductivity by fully *m*-SWCNT paths. This means that these remaining non-functionalized *m*-SWCNTs in the core of the bundles do not form a percolating subnetwork after high functionalization of the bundles. When the *m*-SWCNTs deeply embedded in bundles in the pristine suspension are not accessible to functionalization, they are probably also inaccessible to direct contact with other similar non-functionalized *m*-SWCNTs once the bundles have been spray-deposited as a film.

## 5 Conclusion

Functionalization being selective for *m*-SWCNTs, it brings an efficient mean to tune the *m*/*sc* ratio of SWCNTs in the native blend. We performed a study of the conductivity of functionalized SWCNTs from 4 to 300 K. The goal was to identify the different mechanisms driving the electronic transport in SWCNT materials with progressively increased functionalization. Our analysis reveals that the total conductivity in SWCNT films is a combination of several transport mechanisms.

At low levels of functionalization, the conductivity is mainly due to *m*-SWCNTs, in which the transport is best described by a parallel combination of a semiconducting VRH mechanism and a LL regime, typical for 1D-metals. Our analysis reveals the existence of a percolating subnetwork of *m*-SWCNTs with a LL component associated to large metallic sections of *m*-SWCNTs. At a medium degree (0.2–0.4 mol%), the functionalization destroys the LL component in the *m*-SWCNTs. At higher levels of functionalization, a second VRH regime, corresponding to transport through partially functionalized *sc*-SWCNTs, appears and coexists in parallel with the first VRH mechanism. As a result, at these functionalization levels, the material behaves as a material with the desired semiconducting properties.

We note that a small part of the non-functionalized *m*-SWCNTs is still present in highly functionalized materials, as can be observed by spectroscopy. The fact that we do not see its signature in the electronic transport indicates that these remaining non-functionalized *m*-SWCNTs do not form a percolating subnetwork.

Our approach allows for an insight into the electronic conduction mechanisms in SWCNT films modified by diazo-functionalization. The study of the charge transport mechanisms enabled us to monitor the progressive

transformation of a material with non-functionalized *m*-SWCNTs into a purely semiconducting material. A practical output of the analysis is that it gives information about the minimum value of the functionalization degree necessary to obtain a semiconducting material potentially usable in plastic electronics or thermoelectrics.

**Funding** This work was supported by the Slovak Research and Development Agency under Contract No. APVV-17–0513 and the Slovak Scientific Agency under Contract No. VEGA 1/0461/21. MJ and PC acknowledge the financial support of the French Research Agency ANR (ANR-11-ASTR-013–01) and of CEA Nanoscience program (SChrlMP).

**Data availability** All data generated or analysed during this study are included in this published article [and its supplementary information files].

## Declarations

**Conflict of interest** The authors declare that there is no conflict of interest.

**Open Access** This article is licensed under a Creative Commons Attribution 4.0 International License, which permits use, sharing, adaptation, distribution and reproduction in any medium or format, as long as you give appropriate credit to the original author(s) and the source, provide a link to the Creative Commons licence, and indicate if changes were made. The images or other third party material in this article are included in the article's Creative Commons licence, unless indicated otherwise in a credit line to the material. If material is not included in the article's Creative Commons licence and your intended use is not permitted by statutory regulation or exceeds the permitted use, you will need to obtain permission directly from the copyright holder. To view a copy of this licence, visit <http://creativecommons.org/licenses/by/4.0/>.

## References

1. Yu B, Liu C, Hou P-X, Tian Y, Li S, Liu B, Li F, Kauppinen EI, Cheng H-M (2011) Bulk synthesis of large diameter semiconducting single-walled carbon nanotubes by oxygen-assisted floating catalyst chemical vapor deposition. *J Am Chem Soc* 133:5232–5235. <https://doi.org/10.1021/ja2008278>
2. Pant M, Singh R, Negi P, Tiwari K, Singh Y (2021) A comprehensive review on carbon nano-tube synthesis using chemical vapor deposition. *Mater Today Proc* 46:11250–11253. <https://doi.org/10.1016/j.matpr.2021.02.646>
3. Hur S-H, Kocabas C, Gaur A, Park OO, Shim M, Rogers JA (2005) Printed thin-film transistors and complementary logic gates that use polymer-coated single-walled carbon nanotube networks. *J Appl Phys* 98:114302. <https://doi.org/10.1063/1.2135415>
4. Hugot N, Casademont H, Jouni M, Hanifi N, Darchy L, Azevedo J, Derycke V, Simonato J-P, Celle C, Chenevier P (2016) Gram-scale carbon nanotubes as semiconducting material for highly versatile route of integration in plastic electronics: Gram-scale carbon nanotube as semi-conducting material. *Phys Status Solidi A* 213:183–192. <https://doi.org/10.1002/pssa.201532699>



5. Liu N, Yun KN, Yu H-Y, Shim JH, Lee CJ (2015) High-performance carbon nanotube thin-film transistors on flexible paper substrates. *Appl Phys Lett* 106:103106. <https://doi.org/10.1063/1.4914400>
6. Wu X, Han Y, Zhang X, Lu C (2017) Spirally structured conductive composites for highly stretchable, robust conductors and sensors. *ACS Appl Mater Interfaces* 9:23007–23016. <https://doi.org/10.1021/acsami.7b06256>
7. Cao Y, Brady GJ, Gui R, Rutherglen C, Arnold MS, Zhou C (2016) Radio frequency transistors using aligned semiconducting carbon nanotubes with current-gain cutoff frequency and maximum oscillation frequency simultaneously greater than 70 GHz. *ACS Nano* 10:6782–6790. <https://doi.org/10.1021/acs.nano.6b02395>
8. Park S, Pitner G, Giri G, Koo JH, Park J, Kim K, Wang H, Sinclair R, Wong H-SP, Bao Z (2015) Large-area assembly of densely aligned single-walled carbon nanotubes using solution shearing and their application to field-effect transistors. *Adv Mater* 27:2656–2662. <https://doi.org/10.1002/adma.201405289>
9. Wang M, Jakubka F, Gannott F, Schweiger M, Zaumseil J (2014) Generalized enhancement of charge injection in bottom contact/top gate polymer field-effect transistors with single-walled carbon nanotubes. *Org Electron* 15:809–817. <https://doi.org/10.1016/j.orgel.2014.01.013>
10. Chortos A, Koleilat GI, Pfattner R, Kong D, Lin P, Nur R, Lei T, Wang H, Liu N, Lai Y-C, Kim M-G, Chung JW, Lee S, Bao Z (2016) Mechanically durable and highly stretchable transistors employing carbon nanotube semiconductor and electrodes. *Adv Mater* 28:4441–4448. <https://doi.org/10.1002/adma.201501828>
11. Dhanabalan SC, Dhanabalan B, Chen X, Ponraj JS, Zhang H (2019) Hybrid carbon nanostructured fibers: stepping stone for intelligent textile-based electronics. *Nanoscale* 11:3046–3101. <https://doi.org/10.1039/C8NR07554A>
12. Gentil S, Lalaoui N, Dutta A, Nedellec Y, Cosnier S, Shaw WJ, Artero V, Le Goff A (2017) Carbon-nanotube-supported bio-inspired nickel catalyst and its integration in hybrid hydrogen/air fuel cells. *Angew Chem Int Ed* 56:1845–1849. <https://doi.org/10.1002/anie.201611532>
13. Siljander S, Keinänen P, Ivanova A, Lehmonen J, Tuukkanen S, Kanerva M, Björkqvist T (2019) Conductive cellulose based foam formed 3D shapes—from innovation to designed prototype. *Materials* 12:430. <https://doi.org/10.3390/ma12030430>
14. Wang W, Kumta PN (2010) Nanostructured hybrid silicon/carbon nanotube heterostructures: reversible high-capacity lithium-ion anodes. *ACS Nano* 4:2233–2241. <https://doi.org/10.1021/nn901632g>
15. De Volder MFL, Tawfik SH, Baughman RH, Hart AJ (2013) Carbon nanotubes: present and future commercial applications. *Science* 339:535–539. <https://doi.org/10.1126/science.1222453>
16. Lefebvre J, Ding J, Li Z, Finnie P, Lopinski G, Malenfant PRL (2017) High-purity semiconducting single-walled carbon nanotubes: a key enabling material in emerging electronics. *Acc Chem Res* 50:2479–2486. <https://doi.org/10.1021/acs.accounts.7b00234>
17. Hwang J-Y, Nish A, Doig J, Douven S, Chen C-W, Chen L-C, Nicholas RJ (2008) Polymer structure and solvent effects on the selective dispersion of single-walled carbon nanotubes. *J Am Chem Soc* 130:3543–3553. <https://doi.org/10.1021/ja0777640>
18. Khripin CY, Fagan JA, Zheng M (2013) Spontaneous partition of carbon nanotubes in polymer-modified aqueous phases. *J Am Chem Soc* 135:6822–6825. <https://doi.org/10.1021/ja402762e>
19. Qiu S, Wu K, Gao B, Li L, Jin H, Li Q (2019) Solution-processing of high-purity semiconducting single-walled carbon nanotubes for electronics devices. *Adv Mater* 31:1800750. <https://doi.org/10.1002/adma.201800750>
20. Jain RM, Howden R, Tvrdy K, Shimizu S, Hilmer AJ, McNicholas TP, Gleason KK, Strano MS (2012) Polymer-free near-infrared photovoltaics with single chirality (6,5) semiconducting carbon nanotube active layers. *Adv Mater* 24:4436–4439. <https://doi.org/10.1002/adma.201202088>
21. Balestrieri M, Keita A-S, Duran-Valdeiglesias E, Alonso-Ramos C, Zhang W, Roux XL, Cassan E, Vivien L, Bezugly V, Fediai A, Derycke V, Filoramo A (2017) Polarization-sensitive single-wall carbon nanotubes all-in-one photodetecting and emitting device working at 1.55  $\mu\text{m}$ . *Adv Funct Mater* 27:1702341. <https://doi.org/10.1002/adfm.201702341>
22. Berger FJ, Higgins TM, Rother M, Graf A, Zakharko Y, Allard S, Matthiesen M, Gotthardt JM, Scherf U, Zaumseil J (2018) From broadband to electrochromic notch filters with printed monochiral carbon nanotubes. *ACS Appl Mater Interfaces* 10:11135–11142. <https://doi.org/10.1021/acsami.8b00643>
23. Jurado JP, Dörfling B, Zapata-Arteaga O, Roig A, Mihi A, Campoy-Quiles M (2019) Solar harvesting: a unique opportunity for organic thermoelectrics? *Adv Energy Mater* 9:1902385. <https://doi.org/10.1002/aenm.201902385>
24. Liu Y, Khavrus V, Lehmann T, Yang H, Stepien L, Greifzu M, Oswald S, Gemming T, Bezugly V, Cuniberti G (2020) Boron-doped single-walled carbon nanotubes with enhanced thermoelectric power factor for flexible thermoelectric devices. *ACS Appl Energy Mater* 3:2556–2564. <https://doi.org/10.1021/acs.aem.9b02243>
25. Blackburn JL, Ferguson AJ, Cho C, Grunlan JC (2018) Carbon-nanotube-based thermoelectric materials and devices. *Adv Mater* 30:1704386. <https://doi.org/10.1002/adma.201704386>
26. Schmidt G, Filoramo A, Derycke V, Bourgoin J-P, Chenevier P (2011) Labile diazo chemistry for efficient silencing of metallic carbon nanotubes. *Chem Eur J* 17:1415–1418. <https://doi.org/10.1002/chem.201002441>
27. Darchy L, Hanifi N, Viaila F, Voisin C, Bayle P-A, Genovese L, Celle C, Simonato J-P, Filoramo A, Derycke V, Chenevier P (2014) A highly selective non-radical diazo coupling provides low cost semi-conducting carbon nanotubes. *Carbon* 66:246–258. <https://doi.org/10.1016/j.carbon.2013.08.064>
28. Schmidt G, Gallon S, Esnouf S, Bourgoin J-P, Chenevier P (2009) Mechanism of the coupling of diazonium to single-walled carbon nanotubes and its consequences. *Chem Eur J* 15:2101–2110. <https://doi.org/10.1002/chem.200801801>
29. Wu C, Guan L (2011) Increasing the semiconducting component in transparent conducting films of single-walled carbon nanotubes. *Carbon* 49:3267–3273
30. Wang C, Xu W, Zhao J, Lin J, Chen Z, Cui Z (2014) Selective silencing of the electrical properties of metallic single-walled carbon nanotubes by 4-nitrobenzenediazonium tetrafluoroborate. *J Mater Sci* 49:2054–2062. <https://doi.org/10.1007/s10853-013-7895-3>
31. Lin S, Hilmer AJ, Mendenhall JD, Strano MS, Blankschtein D (2012) Molecular perspective on diazonium adsorption for controllable functionalization of single-walled carbon nanotubes in aqueous surfactant solutions. *J Am Chem Soc* 134:8194–8204
32. Blanch AJ, Lenehan CE, Quinton JS (2012) Dispersant effects in the selective reaction of aryl diazonium salts with single-walled carbon nanotubes in aqueous solution. *J Phys Chem C* 116:1709–1723. <https://doi.org/10.1021/jp208191c>
33. Cognet L, Tsybouski DA, Rocha J-DR, Doyle CD, Tour JM, Weisman RB (2007) Stepwise quenching of exciton fluorescence in carbon nanotubes by single-molecule reactions. *Science* 316:1465–1468. <https://doi.org/10.1126/science.1141316>
34. Bouilly D, Janssen JL, Cabana J, Côté M, Martel R (2015) Graft-induced midgap states in functionalized carbon nanotubes. *ACS Nano* 9:2626–2634. <https://doi.org/10.1021/nn506297z>
35. López-Bezanilla A, Triozon F, Latil S, Blase X, Roche S (2009) Effect of the chemical functionalization on charge transport in carbon

- nanotubes at the mesoscopic scale. *Nano Lett* 9:940–944. <https://doi.org/10.1021/nl802798q>
36. Buldum A, Lu JP (2001) Contact resistance between carbon nanotubes. *Phys Rev B* 63:161403
  37. Stadermann M, Papadakis SJ, Falvo MR, Novak J, Snow E, Fu Q, Liu J, Fridman Y, Boland JJ, Superfine R, Washburn S (2004) Nanoscale study of conduction through carbon nanotube networks. *Phys Rev B* 69:2011402
  38. Tuukkanen S, Streiff S, Chenevier P, Pinault M, Jeong H-J, Enouz-Vedrenne S, Cojocar CS, Pribat D, Bourgoin J-P (2009) Toward full carbon interconnects: High conductivity of individual carbon nanotube to carbon nanotube regrowth junctions. *Appl Phys Lett* 95:113108. <https://doi.org/10.1063/1.3216839>
  39. Kim DH, Huang J, Shin HK, Roy S, Choi W (2006) Transport phenomena and conduction mechanism of single-walled carbon nanotubes (SWNTs) at Y- and crossed-junctions. *Nano Lett* 6:2821–2825
  40. Bandaru PR (2007) Electrical characterization of carbon nanotube Y-junctions: a foundation for new nanoelectronics. *J Mater Sci* 42:1809–1818
  41. Kyrlyuk AV, Hermant MC, Schilling T, Klumperman B, Koning CE, van der Schoot P (2011) Controlling electrical percolation in multicomponent carbon nanotube dispersions. *Nat Nano* 6:364–369
  42. Ponzoni A (2019) The contributions of junctions and nanowires/nanotubes in conductive networks. *Appl Phys Lett* 114:153105. <https://doi.org/10.1063/1.5090117>
  43. Yanagi K, Udoguchi H, Sagitani S, Oshima Y, Takenobu T, Kataura H, Ishida T, Matsuda K, Maniwa Y (2010) Transport mechanisms in metallic and semiconducting single-wall carbon nanotube networks. *ACS Nano* 4:4027–4032. <https://doi.org/10.1021/nn101177n>
  44. Bulmer JS, Lekawa-Raus A, Rickel DG, Balakirev FF, Kozioł KK (2017) Extreme magneto-transport of bulk carbon nanotubes in sorted electronic concentrations and aligned high performance fiber. *Sci Rep* 7:12193. <https://doi.org/10.1038/s41598-017-12546-6>
  45. Itkis ME, Pekker A, Tian X, Bekyarova E, Haddon RC (2015) Networks of semiconducting SWNTs: contribution of midgap electronic states to the electrical transport. *Acc Chem Res* 48:2270–2279. <https://doi.org/10.1021/acs.accounts.5b00107>
  46. Wang X, Gao W, Li X, Zhang Q, Nanot S, Hároz EH, Kono J, Rice WD (2018) Magnetotransport in type-enriched single-wall carbon nanotube networks. *Phys Rev Mater* 2:116001. <https://doi.org/10.1103/PhysRevMaterials.2.116001>
  47. Kaiser AB, Skákalová V (2011) Electronic conduction in polymers, carbon nanotubes and graphene. *Chem Soc Rev* 40:3786. <https://doi.org/10.1039/c0cs00103a>
  48. Skákalová V, Kaiser AB, Woo Y-S, Roth S (2006) Electronic transport in carbon nanotubes: from individual nanotubes to thin and thick networks. *Phys Rev B* 74:085403. <https://doi.org/10.1103/PhysRevB.74.085403>
  49. Vavro J, Kikkawa JM, Fischer JE (2005) Metal-insulator transition in doped single-wall carbon nanotubes. *Phys Rev B* 71:155410. <https://doi.org/10.1103/PhysRevB.71.155410>
  50. Sheng P (1980) Fluctuation-induced tunneling conduction in disordered materials. *Phys Rev B* 21:2180
  51. Lee PA, Ramakrishnan TV (1985) Disordered electronic systems. *Rev Mod Phys* 57:287–337. <https://doi.org/10.1103/RevModPhys.57.287>
  52. Larkin AI, Khmel'nitskii DE (1982) Activation conductivity in disordered systems with large localization lengths. *Sov Phys JETP* 56:647–652
  53. Egger R (1999) Luttinger liquid behavior in multiwall carbon nanotubes. *Phys Rev Lett* 83:5547
  54. Yao Z, Postma HWC, Balents L, Dekker C (1999) Carbon nanotube intramolecular junctions. *Nature* 402:273–276. <https://doi.org/10.1038/46241>
  55. Postma HWC, Teepe T, Yao Z, Grifoni M, Dekker C (2001) Carbon nanotube single-electron transistors at room temperature. *Science* 293:76–79. <https://doi.org/10.1126/science.1061797>
  56. Ravi S, Kaiser AB, Bumby CW (2010) Improved conduction in transparent single walled carbon nanotube networks drop-cast from volatile amine dispersions. *Chem Phys Lett* 496:80–85. <https://doi.org/10.1016/j.cplett.2010.06.084>
  57. Mott NF, Davis EA (1979) *Electronic processes in non crystalline materials*. Oxford, New York
  58. Efros AL, Shklovskii BI (1987) Influence of electron-electron interaction on hopping conduction of disordered systems. *J Non-Cryst Solids* 97–98:31–38. [https://doi.org/10.1016/0022-3093\(87\)90010-X](https://doi.org/10.1016/0022-3093(87)90010-X)
  59. Zabrodskii AG (1980) Electrical conductivity of heavily doped compensated n-type germanium produced by neutron doping. *Sov Phys Semicond* 14:670–676
  60. Skotheim TA, Reynolds JR (eds) (2007) *Handbook of conducting polymers. Conjugated polymers: theory, synthesis, properties, and characterization*, 3rd edn. CRC Press, Boca Raton
  61. Sasso C, Bruyant N, Beneventi D, Faure-Vincent J, Zeno E, Petit-Conil M, Chaussy D, Belgacem MN (2011) Polypyrrole (PPy) chemical synthesis with xylan in aqueous medium and production of highly conducting PPy/nanofibrillated cellulose films and coatings. *Cellulose* 18:1455–1467. <https://doi.org/10.1007/s10570-011-9583-2>
  62. Dini Y, Faure-Vincent J, Dijon J (2019) How to overcome the electrical conductivity limitation of carbon nanotube yarns drawn from carbon nanotube arrays. *Carbon* 144:301–311. <https://doi.org/10.1016/j.carbon.2018.12.041>
  63. Dini Y, Rouchon D, Faure-Vincent J, Dijon J (2020) Large improvement of CNT yarn electrical conductivity by varying chemical doping and annealing treatment. *Carbon* 156:38–48. <https://doi.org/10.1016/j.carbon.2019.09.022>
  64. Foroughi J, Spinks GM, Ghorbani SR, Kozlov ME, Safaei F, Peleckis G, Wallace GG, Baughman RH (2012) Preparation and characterization of hybrid conducting polymer–carbon nanotube yarn. *Nanoscale* 4:940–945. <https://doi.org/10.1039/C2NR11580H>
  65. Dini Y, Faure-Vincent J, Dijon J (2020) A unified electrical model based on experimental data to describe electrical transport in carbon nanotube-based materials. *Nano Res* 13:1764–1779. <https://doi.org/10.1007/s12274-020-2803-z>
  66. Jouni M, Faure-Vincent J, Fedorko P, Djurado D, Boiteux G, Massardier V (2014) Charge carrier transport and low electrical percolation threshold in multiwalled carbon nanotube polymer nanocomposites. *Carbon* 76:10–18. <https://doi.org/10.1016/j.carbon.2014.04.031>
  67. Jemai G, Khabthani JJ, de Laissardière GT, Mayou D (2019) Quantum localization and electronic transport in covalently functionalized carbon nanotubes. *J Phys Condens Matter* 32:115301. <https://doi.org/10.1088/1361-648X/ab5a2d>
  68. Bockrath M, Cobden DH, Lu J, Rinzler AG, Smalley RE, Balents L, McEuen PL (1999) Luttinger-liquid behaviour in carbon nanotubes. *Nature* 397:598–601. <https://doi.org/10.1038/17569>
  69. Kane C, Balents L, Fisher MP (1997) Coulomb interactions and mesoscopic effects in carbon nanotubes. *Phys Rev Lett* 79:5086
  70. Jeong H, Park J-Y (2015) Local electrical investigations of nitric acid treatment effects on carbon nanotube networks. *J Phys Chem C* 119:9665–9668. <https://doi.org/10.1021/acs.jpcc.5b02633>

71. Stern A, Azoubel S, Sachyani E, Livshits GI, Rotem D, Magdassi S, Porath D (2018) Conductivity enhancement of transparent 2D carbon nanotube networks occurs by resistance reduction in all junctions. *J Phys Chem C* 122:14872–14876. <https://doi.org/10.1021/acs.jpcc.8b01215>

**Publisher's Note** Springer Nature remains neutral with regard to jurisdictional claims in published maps and institutional affiliations.